This is a repository copy of *EMBlast: A software for calculating blast loads on structures from the detonation of energetic materials*.

White Rose Research Online URL for this paper:
https://eprints.whiterose.ac.uk/194753/

Version: Published Version

Article:
Angelides, S.C., Burgan, B.A., Kyprianou, C. et al. (2 more authors) (2022) EMBlast: A software for calculating blast loads on structures from the detonation of energetic materials. Fire and Blast Information Group Technical Newsletter (85). pp. 19-25.

© 2022 FABIG. Reproduced here by permission of the publisher. For reuse permissions please contact FABIG.

Reuse
Items deposited in White Rose Research Online are protected by copyright, with all rights reserved unless indicated otherwise. They may be downloaded and/or printed for private study, or other acts as permitted by national copyright laws. The publisher or other rights holders may allow further reproduction and re-use of the full text version. This is indicated by the licence information on the White Rose Research Online record for the item.

Takedown
If you consider content in White Rose Research Online to be in breach of UK law, please notify us by emailing eprints@whiterose.ac.uk including the URL of the record and the reason for the withdrawal request.

eprints@whiterose.ac.uk
https://eprints.whiterose.ac.uk/

EMBlast: A SOFTWARE FOR CALCULATING BLAST LOADS ON STRUCTURES FROM THE DETONATION OF ENERGETIC MATERIALS

Written by:
S.C. Angelides[1,2], B.A. Burgan[1], C. Kyprianou[1], S.E. Rigby[2], A. Tyas[2]
[1]**Steel Construction Institute, UK**
[2]**University of Sheffield, UK**

1 Introduction

Industrial structures located nearby explosive storage facilities are at risk from the stored materials accidentally detonating. Such was the case in the 2011 damage of the Vasilikos Power Plant in Cyprus, following the accidental explosion 300-500 m away from the Naval Base E. Florakis that was temporarily storing ammunition intercepted from a cargo ship. The majority of the structures located in the power plant collapsed, resulting in severe financial losses, including the shut-down of the power plant that at the time produced 70% of Cyprus' electricity [1]. Urbanisation has increased the risk of accidental explosions occurring, as many industrial structures are now located near petrochemical, chemical and explosive storage facilities. This was the case in the 2020 accidental explosion occurring at the Port of Beirut that resulted in the damage of various industrial structures, as well as residential and commercial buildings [2].

Current software for calculating blast loads on structures from the detonation of energetic materials are either general-purpose computational fluid dynamics (CFD) software or restricted fast-running software originating from the US military. The former are expensive, complex and computationally very demanding. The latter are often restricted to use on US Government contracts; this means that copies in use elsewhere are without documentation (hence used as 'black boxes'), not up-to-date and not compatible with modern IT systems. As a direct response to industry and government requests, this research project aims to develop new tools for predicting accurately and fast, but simplified presented, the loading on structures following an explosion. The outcome of this research is then implemented into EMBlast, a blast loading prediction software that can assist practitioners in the blast design of structures. EMBlast can also be used to assess the blast performance of buildings at risk from a terrorist attack by predicting the blast loads on façades that act as the first barrier of defence during an external explosion [3]. This paper will present the theoretical background of these tools, including a description of the predicted free-field and reflected pressure-time histories.

2 Model description

To derive the pressure-time history at a target (A) following the detonation of an energetic material, three input parameters are required: the explosive weight *W*, the range between the target and the charge R_A and the charge position relative to the ground surface. These input parameters are required to define the scaled distance *Z*, given by Equation (1), that governs the free-field (denoted with the subscript 'so') and reflected (denoted with the subscript 'r') blast parameters shown in Figure 1:

$$Z = \frac{R_A}{W^{1/3}} \quad (1)$$

The blast parameters include the blast wave time of arrival t_a, positive t_d and negative t^-_d phase durations, peak positive free field P_{so} and reflected P_r pressures, peak negative free field P^-_{so} and reflected P^-_r pressures, positive free field i_{so} and reflected i_r impulses, and free field i^-_{so} and reflected i^-_r negative impulses. The free-field parameters refer to incident (i.e. side-on) pressure-time histories at a target point, without accounting for reflection on a target surface. The reflected

blast wave parameters account for the reflection on a target surface and therefore, result in amplified pressure-time histories, as shown in Figure 1. The derivation of these parameters and the subsequent construction of the resulting pressure-time history at a target point are discussed in Sections 3 and 4.

The weight of an explosive considered in the scaled distance formula depends on the type of the explosive. The TNT equivalence factors for pressure and impulse specified in ISO/FDIS 16933 [4] are used to convert the weight of various explosive types to TNT equivalent weights. As shown in Figure 2, three different types of bursts are considered: spherical free-air burst, hemispherical surface burst (soft and hard ground) and spherical above ground burst. These indicate the location of a charge with respect to the ground, in order to account for reflection effects on the ground. In the former configuration, the charge is assumed to be located at significant distance from the ground. Therefore, ground reflection effects are ignored, with the analysis considering only the incident spherical blast waves originating from the explosive location. In the latter two configurations, ground reflection effects are considered in the analysis. These are discussed in more detail Sections 3 and 4.

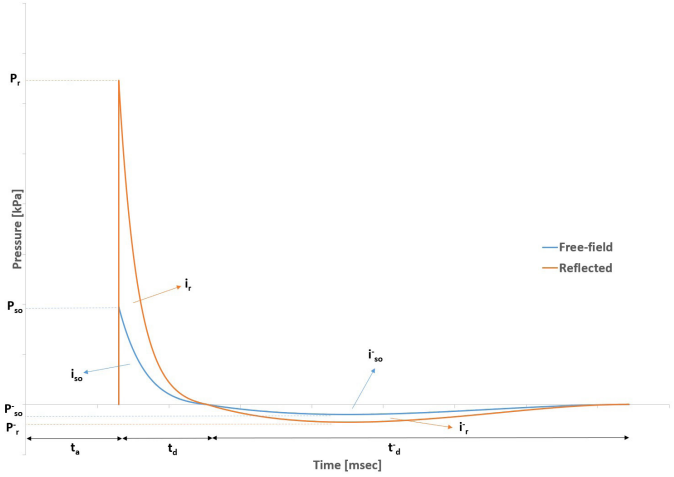

Figure 1 Pressure time-history at a target point, indicating the free-field and reflected blast parameters

3 Free-field blast wave parameters

The methodology for deriving the blast parameters and the subsequent pressure-time histories varies for each of the three burst types introduced in Section 2. These are discussed separately in the following sub-sections.

3.1 Free-air bursts

For free-air bursts, the **positive phase** pressure-time history $p_{so}(t)$ at a target point (A) is described by the modified Friedlander expression, given by Equation (2):

$$p_{so}(t) = P_{so}\left[1 - \frac{t}{t_d}\right] e^{-\frac{bt}{t_d}} \quad (2)$$

where, P_{so} is the peak pressure, t is the time, t_d is the positive time duration and b is the decay factor.

For scaled distances up to 40 $\mathrm{m/kg^{1/3}}$, the time of arrival t_a, peak pressure P_{so}, impulse i_{so} and positive phase duration t_d are derived from polynomial equations fitted to free-air burst (spherical charges) blast trials [5]. These polynomial equations have been implemented in military standards and are included in the appendix of UFC 3-340 01 [6] and presented in the form of graphs in UFC 3-340-02 [7]. The decay factor b is calculated iteratively by setting the integral of the modified Friedlander equation to be equal to the impulse value i_{so}.

For scaled distances greater than 40 $\mathrm{m/kg^{1/3}}$ up to 100 $\mathrm{m/kg^{1/3}}$, the peak pressure P_{so} and impulse i_{so} are derived from polynomial equations [8] fitted to far-field surface burst (hemispherical charges) blast trials [9]. To convert the surface charge polynomials to equivalent free-air charge, the charge weight is divided by a 1.7 factor that removes the ground amplification effect (this assumes soft ground conditions, for hard ground conditions the charge weight would be divided by a factor of 2). The modified free-air polynomials are compared with numerical far-field CFD predictions identified in the literature (ALE3D [10]) and independently performed (Viper),

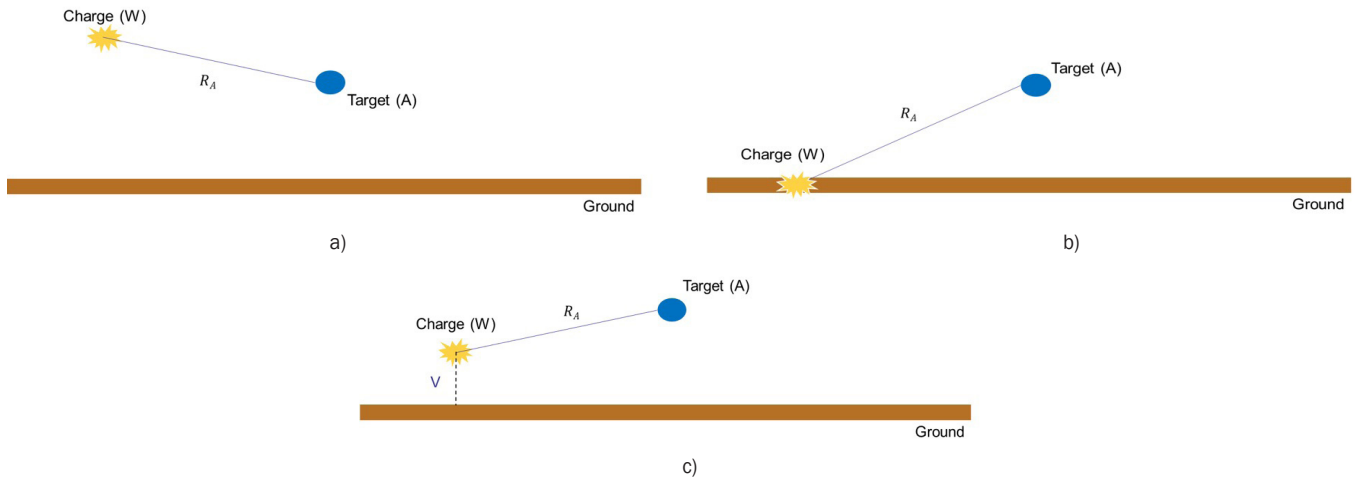

Figure 2 Three different types of bursts: a) Free-air, b) Surface (soft and hard ground) and c) Above-ground

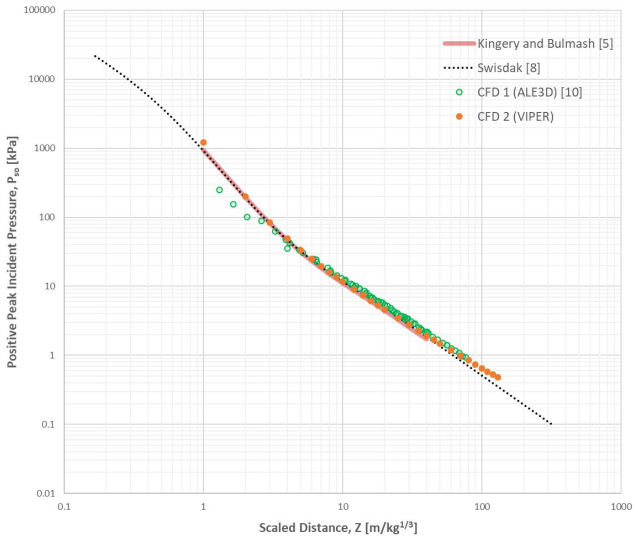

a)

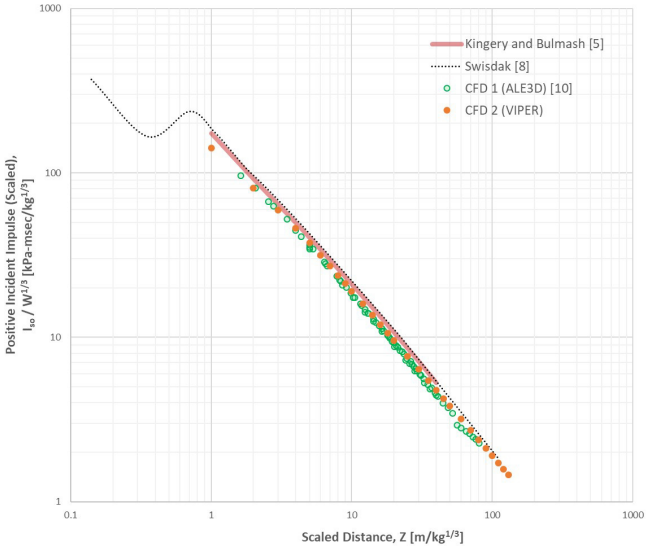

b)

Figure 3 Comparison of polynomial equations fitted to blast trials (mid-field [5] and far-field [8]) with CFD predictions (ALE3D [10] and Viper): a) peak positive pressure P_{so}, b) positive scaled impulse i_{so} / $W^{1/3}$

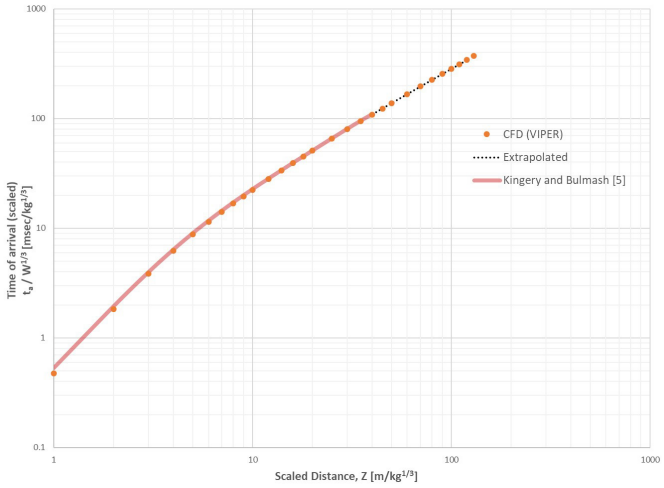

Figure 4 Comparison of CFD predictions (Viper) for the scaled time of arrival t_a / $W^{1/3}$ with extrapolation of polynomial equations (fitted to mid-field blast trials [5]) to the far-field

as shown in Figure 3. The time of arrival t_a of the blast waves in the far-field is calculated from a linear extrapolation of the time of arrival t_a at a scaled distance of 40 $\mathrm{m/kg^{1/3}}$. In this extrapolation, a constant wave front velocity of 343 m/s is assumed (the velocity converges to this value in the far-field, as can be seen from the polynomial equations [5]). Figure 4 compares the extrapolated time of arrival t_a values in the far-field with CFD predictions (Viper). As the decay factor approaches zero at scaled distance of 40 $\mathrm{m/kg^{1/3}}$, a linear relationship is assumed for the positive phase pressure-time history at greater scaled distances. The positive phase duration t_d is then calculated by setting the integral of the modified Friedlander equation to be equal to the impulse value i_{so}, as given by Equation (3).

$$t_d = \frac{2i_{so}}{P_{so}} \qquad (3)$$

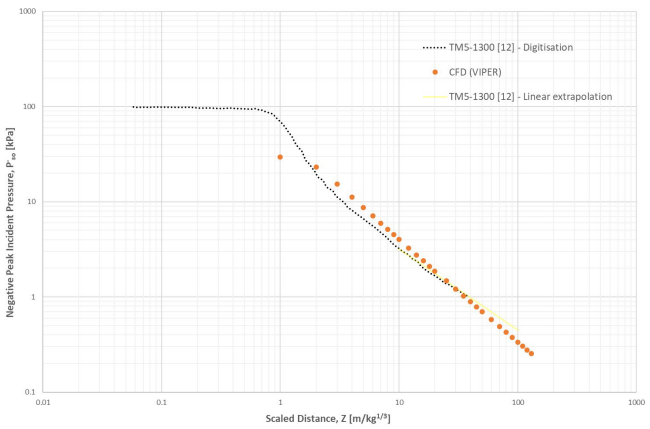

a)

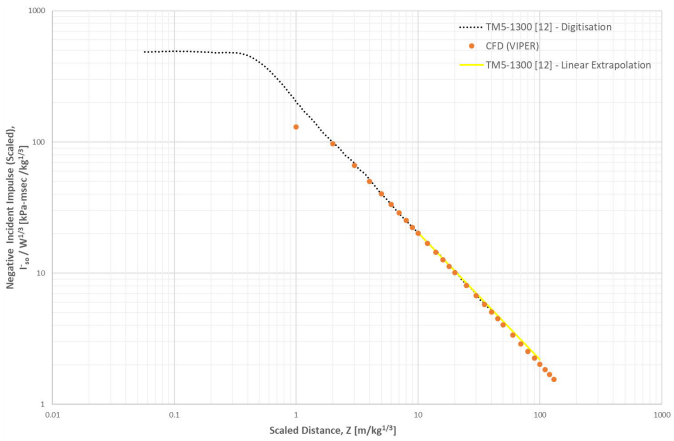

b)

Figure 5 Comparison of digitisation and linear extrapolation of Figure 2.8 in TM5-1300 [12] with CFD predictions (Viper): a) peak negative pressure P^-_{so}, b) negative scaled impulse i^-_{so} / $W^{1/3}$

The **negative** phase pressure-time history $p_{so}^{-}(t)$ at a target point (A) is described by the cubic expression provided in [11] and replicated here as Equation (4):

$$p_{so}^{-}(t) = -P_{so}^{-}\left(\frac{6.75(t-t_d)}{t_d^{-}}\right)\left(1-\frac{(t-t_d)}{t_d^{-}}\right)^2 \qquad t_d < t \le t_d + t_d^{-} \quad (4)$$

where, P^{-}_{so} is the negative peak pressure, t is the time, t_d is the positive time duration and t_d^{-} is the negative time duration.

For scaled distances up to $40\,\mathrm{m/kg^{1/3}}$, the negative peak pressure P^{-}_{so} and impulse i^{-}_{so} are derived from Figure 2.8 in TM5-1300 [12] (includes data points for greater scaled distances compared to its more recent revision, UFC 3-340-02 [7]), as polynomial equations are not available for the negative phase. This figure has been digitised and linearly extrapolated to scaled distances greater than $40\,\mathrm{m/kg^{1/3}}$ and up to $100\,\mathrm{m/kg^{1/3}}$. The digitisation and extrapolation are shown in Figure 5, together with CFD comparisons (from Viper). The duration t^{-}_{d} is calculated iteratively by setting the integral of the cubic expression equation to be equal to the impulse value i^{-}_{so}.

3.2 Surface bursts

The blast parameters for soft ground surface bursts are derived from surface burst (hemi-spherical charges) blast trials. For scaled distances up to $40\ \mathrm{m/kg^{1/3}}$, polynomial equations [5] and Figure 2.16 in TM5-1300 [12] are implemented for the positive and negative phase, respectively. To extend the blast parameters to scaled distances greater than $40\ \mathrm{m/kg^{1/3}}$ and up to $100\ \mathrm{m/kg^{1/3}}$, similar calculations to those described in Section 3.1 for the free-air bursts are performed. The hard ground surface burst blast parameters are derived from the free-air burst parameters. However, a modified scaled distance is considered with double the charge weight ($2W$) to account for the ground amplification, given in Equation (5):

$$Z = \frac{R_A}{(2W)^{1/3}} \quad (5)$$

3.3 Above-ground bursts

In above ground bursts, there are two reflection regimes in the space surrounding a target point. When a blast wave comes into contact with the ground its reflection creates a second wave i.e. the ground-reflected wave. In the first regime, the incident and ground-reflected waves meet at the target. In the second, the reflected wave is able to catch up with the incident wave and a single combined wave is formed near the ground. This is called the Mach reflection region and the merged wave is called the Mach stem. The point at which the incident, reflected and Mach waves intersect is called the triple-point. Collectively, all points are referred to as the triple-point path.

When the target is located **below the triple-point path** (i.e. in the Mach region), the combined effects of the incident and the ground-reflected waves are applied to the target point. Therefore, the peak Mach incident pressure at a target point (A) is calculated by multiplying the peak incident pressure P_{so} (i.e. without accounting for the ground-reflected wave contributions) with a reflection coefficient C_r that accounts for the ground-reflection amplification. Following the UFC 3-340-02 [7] methodology, a modified range R', between the charge and the projection of the target point on the ground, is considered in the calculation of the scaled distance for establishing the peak incident pressure P_{so} from the empirical polynomials for a free-air bust. However, instead of assuming a normal projection as in UFC 3-340-02 [7], an arc with its centre at the projection point of the charge on the ground is drawn, such that the arc passes through the target point. It is assumed that all points on this arc have the same peak incident pressure as the intersection point of the arc with the ground. Similar assumptions can also be found in the literature [13]. The UFC 3-340-02 [7] assumption of a straight Mach Stem is more appropriate for far-field nuclear detonations, where the range is considered large compared to the height of a building. Finally, to improve the agreement with CFD analyses, a new modified range R'' between the charge and the intersection of the arc with the triple-point path is considered for calculating the time of arrival t_a of the Mach wave at a target point (A). The two modified ranges R' and R'', considered in the derivation of the blast parameters, are shown graphically in Figure 6a.

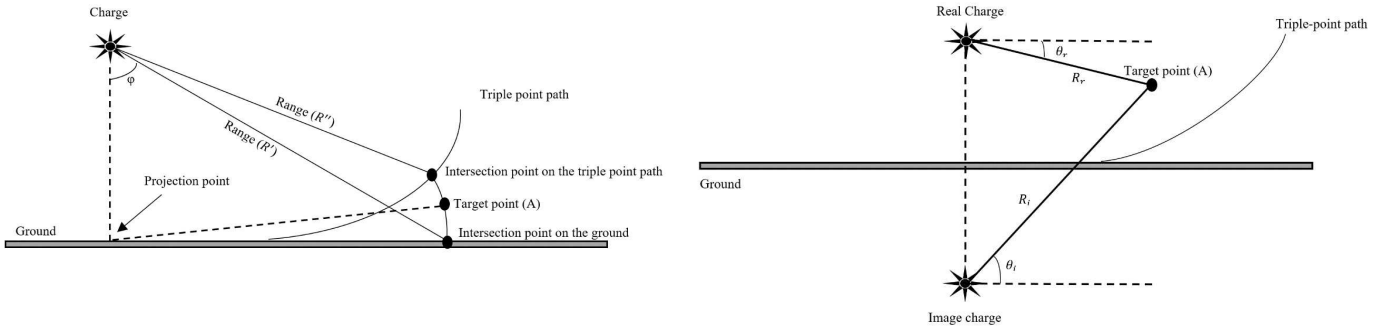

Figure 6 Above ground burst methodology:
a) Modified ranges for target points below the triple point path and b) LAMB combination for target points above the triple point path

When the target is located **above the triple-point path**, the incident and the ground-reflected waves arrive separately at the target point. Due to nonlinear effects at high pressures, a non-linear superposition of the blast waves is required. Therefore, the two waves are combined using the Low Altitude Multiple Burst (LAMB) shock addition rules. This is a semi-empirical method based on the conservation of mass, momentum, and energy that was initially developed for nuclear detonations [14]. In this methodology, it is assumed that a ground-reflected wave is created by a fictitious charge (image) of identical weight to the actual charge (real) and located below the ground at the same distance as the actual charge above the ground (refer to Figure 6b).

4 Reflected blast wave parameters

This section presents the methodology for calculating reflected pressure-time histories on infinite and finite target surfaces.

4.1 Infinite target surfaces

Exiting polynomial equations fitted to blast trial results are used for calculating the reflected blast parameters [5, 8]. These are also implemented in military standards [6, 7] and are limited to a scaled distance of 40 $\mathrm{m/kg^{1/3}}$. Therefore, the LAMB methodology (introduced in Section 3) is applied to extend the reflected pressure-time history up to a scaled distance of 100 $\mathrm{m/kg^{1/3}}$ by combining the incident and target-reflected wave pressure-time histories. The reflected impulses (i_r, i_r^-) are calculated by integrating the reflected pressure-time history. The free-field blast parameters derived in Section 3 are assumed for the durations (t_d, t_d^-) and time of arrival t_a. In the LAMB methodology, the target-reflected wave is assumed to originate from a fictitious charge (image) of identical weight to the actual charge (real) and located at the same normal distance, D, from the target surface as the real charge, but on the opposite side of the target surface. Therefore, the range between both charges and any target point is the same, i.e. $R_r = R_i$. This is shown graphically in Figure 7 for above-ground burst configurations. The LAMB predictions for the peak reflected pressures P_r are compared in Figure 8 with the polynomial equations [5], [8] and CFD (Viper) simulations, in the mid- and far-field, respectively.

For above-ground bursts with targets located **below the triple-point path**, a merged wave centre on the ground (i.e. normal projection from the real charge location on the ground) is assumed. This merged wave centre simulates the origin of the Mach wave, which accounts for the combined effect of the incident and ground-reflected waves, as previously discussed in Section 3. Therefore, to account for the reflection on the target area, an image of the merged wave centre is placed on the ground on the opposite side of the target surface, as shown in Figure 7a. To derive the reflected pressure time-history on a target located **above the triple-point path** for above-ground bursts, four charges are created. These include the real charge

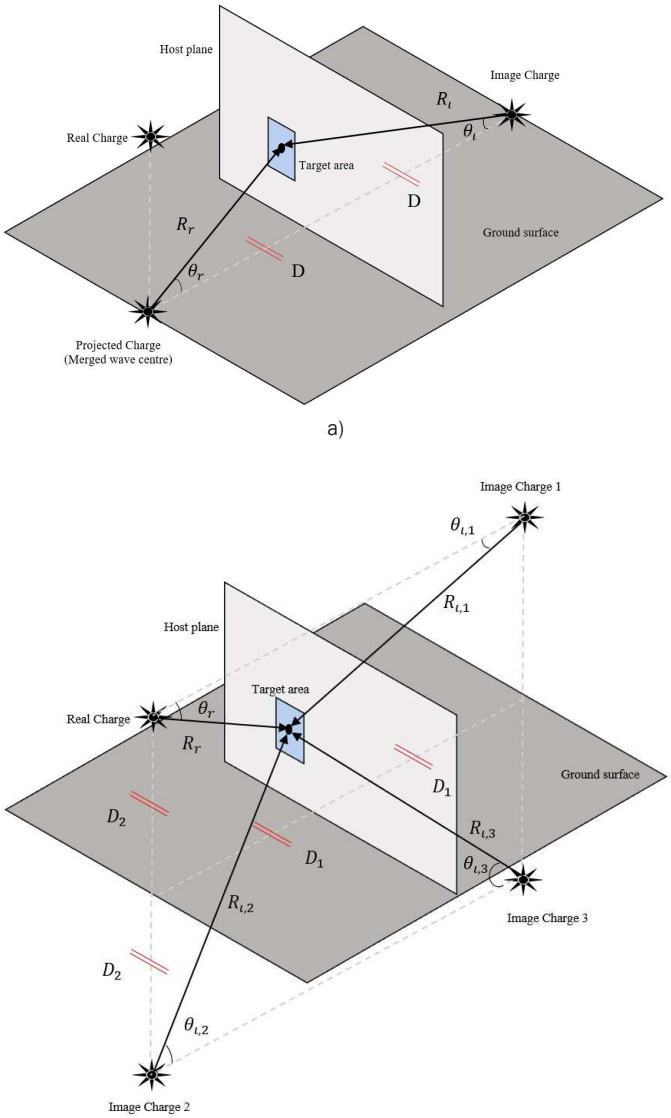

Figure 7 LAMB methodology for calculating reflected pressure-time histories on a target surface for an above-ground burst configuration: a) target below triple-point path, b) target above triple-point path

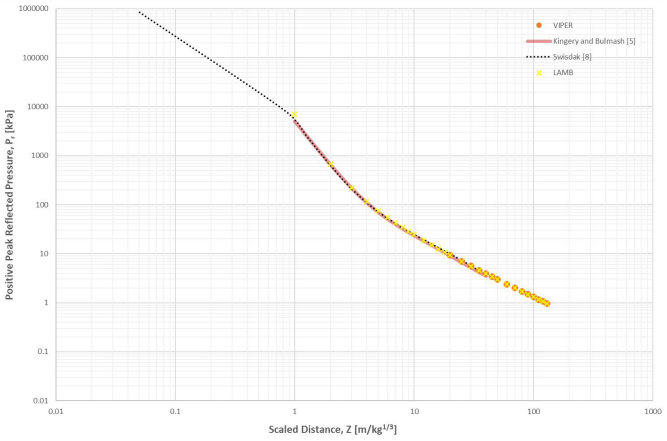

Figure 8 Comparison of polynomial equations fitted to blast trials [5, 8], CFD predictions (Viper) and LAMB calculations for the peak positive pressure P_r

and three image charges, as shown in Figure 7b. Image charge 1 is created to account for the target-reflection of the real charge, image charge 2 accounts for the ground-reflection of the real charge and image charge 3 accounts for the target-reflection of the ground-reflected wave. The ranges between the real charge and image charge 1 to any target point are equal (i.e. $R_r = R_{i,1}$). The same also applies for the ranges between image charges 2 and 3 to any target point (i.e. $R_{i,2} = R_{i,3}$).

4.2 *Finite target surfaces*

The reflected pressure-time histories derived using the LAMB methodology correspond to an infinitely large structure. For structures of finite size, these reflected pressures are reduced due to clearing effects, a phenomenon that results in gradually reducing the reflected pressures of the front face of a structure, with respect to the charge location, to the lower free-field pressures experienced by the sides and roof. The reduced reflected pressure-time history is calculated using the Hudson method [15]. This is a first-principles approach to account for clearing effects by superimposing the reflected pressure-time history calculated at target point (A) with pressure relief waveforms travelling from the edges of the surface of the structure (x_A and y_A shown in Figure 9a). The combined pressure-time history experienced by target point (A) is shown in Figure 9b. This method has shown good agreement with experimental and numerical results in the mid- and far-field [16, 17].

5 Conclusions

This paper has presented methods for rapidly and accurately predicting blast loads on structures. These tools are implemented in EMBlast, a blast load prediction software that practitioners can use to design structures and assess their blast performance. The free-field and reflected blast parameters, which are required for deriving the resulting pressure-time history on a target, are calculated from a combination of polynomial equations fitted to blast trial results and semi-empirical methods. Compared to existing military standards that are limited to a scaled distance of 40 $\mathrm{m/kg^{1/3}}$, the developed tools are also applicable in the far-field, up to a scaled distance of 100 $\mathrm{m/kg^{1/3}}$. The predictions of the blast parameters are validated with numerical computational fluid dynamics simulations. Future work will focus on expanding the clearing predictions on target surfaces in the near-field, where the shock front is less likely to be planar and semi-analytical methods, such as the Hudson method, are less likely to yield accurate predictions. Additionally, an entire new module focusing on internal explosions will be explored, focusing on the detonation of energetic materials taking place in confined spaces.

6 Acknowledgements

The authors gratefully acknowledge Innovate UK for funding this research through a Knowledge Transfer Partnership (KTP). The authors also wish to thank Colin Morison from ColMor Consultancy Ltd for providing guidance and CFD Viper results.

This paper was presented at the CICIND 97th Conference in Paphos, October 21, 2022.

References

[1] M. Angelides, “The July 2011 Explosion in Cyprus and its Impact on the Vasilikos Power Plant,” in CICIND 97th Conference, Paphos, 2022.

[2] S. E. Rigby, T. J. Lodge, S. Alotaibi, A. D. Barr, S. D. Clarke, G. S. Langdon and A. Tyas , “Preliminary yield estimation of the 2020 Beirut explosion using video footage from social media,” Shock Waves, vol. 30, p. 671–675, 2020. https://doi.org/10.1007/s00193-020-00970-z

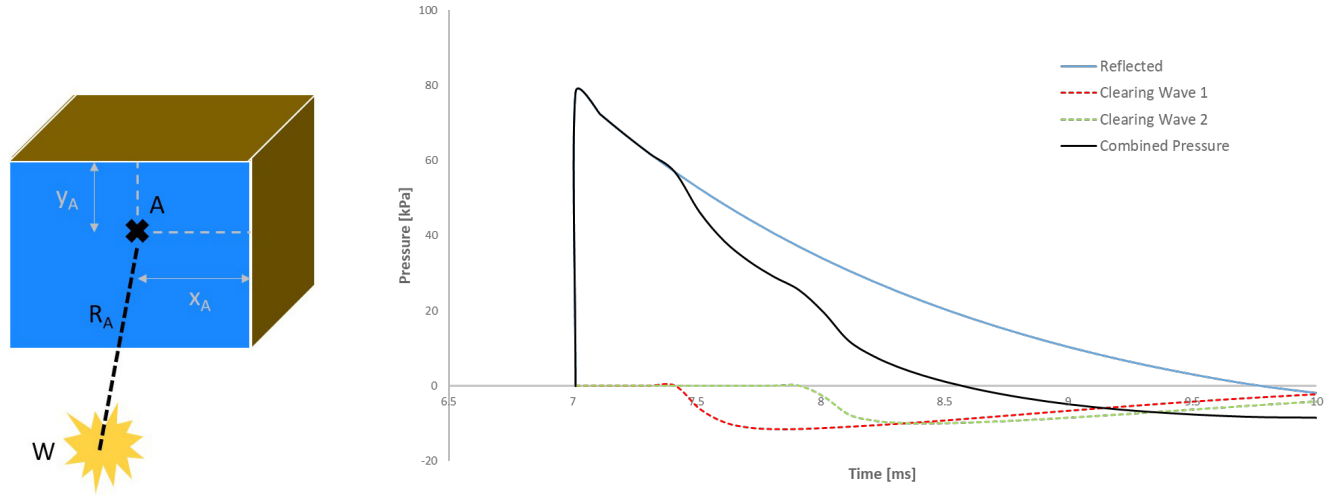

a) b)

Figure 9 a) Location of target point (A) on a finite surface, b) Resulting pressure-time history on target point (A) accounting for clearing effects

[3] S. C. Angelides and J. P. Talbot, "Blast response of laminated glass panels: a critical review of analysis and design methods," Proceedings of the Institution of Civil Engineers – Structures and Buildings, 2022. https://doi.org/10.1680/jstbu.20.00248

[4] "ISO 16933:2007 Glass in building — Explosion-resistant security glazing — Test and classification for arena air-blast loading," ISO, 2007.

[5] C. N. Kingery and G. Bulmash, "ARBRL-TR-02555 Airblast Parameters from TNT Spherical Air Burst and Hemispherical Surface Burst," 1984.

[6] "UFC 3-340-01 Design And Analysis Of Hardened Structures To Conventional Weapons Effects.".

[7] "UFC 3-340-02 Structures to Resist the Effects of Accidental Explosives".

[8] M. M. Swisdak Jr., "Simplified Kingery Airblast Calculations," 1994.

[9] C. N. Kingery and B. F. Pannill, "AD443102 Peak Overpressure Vs Scaled Distance for TNT Surface Bursts (Hemispherical Charges)," 1964.

[10] A. G. Taylor, "Numerical Analysis of Blast Effects and Mitigation in the Far-Field from Small Explosions," Applied Sciences, vol. 12, no. 8824, 2022. https://doi.org/10.3390/app12178824

[11] S. Rigby, A. Tyas, T. Bennett, S. D. Clarke and S. D. Fay, "The Negative Phase of the Blast Load," International Journal of Protective Structures, vol. 5, no. 1, p. 1–19, 2014. https://doi.org/10.1260/2041-4196.5.1.1

[12] "TM5-1300 Structures to Resist the Effects of Accidental Explosions".

[13] C. E. Needham, Blast Waves, 2nd ed., Cham, Switzerland: Springer, 2018.

[14] S. Hikida and C. E. Needham, "Low Altitude Multiple Burst (LAMB) Model: Volume I - Shock Description," 1981.

[15] S. Rigby, "Blast Wave Clearing Effects on Finite-Sized Targets Subjected to Explosive Loads," University of Sheffield, Sheffield, UK, 2014.

[16] A. Tyas, J. A. Warren, T. Bennett and S. Fay, "Prediction of clearing effects in far-field blast loading of finite targets," Shock Waves, vol. 21, p. 111–119, 2011. https://doi.org/10.1007/s00193-011-0308-0

[17] M. K. Nartu, M. Kumar and S. B. Ramisetti, "Improved Methodology for Accurate Prediction of Blast Wave Clearing on a Finite Target," Journal of Engineering Mechanics, vol. 148, no. 9, 2022. https://doi.org/10.1061/(ASCE)EM.1943-7889.0002134

For further information, please contact:

Dr. Socrates Angelides
The Steel Construction Institute
E: s.angelides@steel-sci.com
W: www.steel-sci.com